Semianalytic Integral Method for Fast Solution of Current Distribution in Foil Winding Transformers

Guillermo Diaz[1] and Enrique Mombello[2]

[1]Universidad de La Salle, Bogotá 110231, Colombia
[2]Universidad Nacional de San Juan, San Juan J5400ARL, Argentina

A novel mesh-free axisymmetric methodology for the determination of the low-frequency current distribution in foil windings is presented in this paper. The proposed methodology applies equivalent models for the foil winding and the iron core, which are based on the field produced by elementary geometric configurations and boundary conditions derived from Maxwell's equations. Power losses in the windings due to skin effect and proximity effect are calculated with the proposed method and the finite-element method (FEM). The comparison of both results showed excellent agreement. The computational performance is also compared with FEM. It has been found that the proposed method achieves significant improvements in computational times compared with FEM retaining the level of precision required for transformer design purposes.

Index Terms— **Finite-element method (FEM), integral methods, proximity effect, sheet current, skin depth, skin effect.**

I. Introduction

THE accurate calculation of the current distribution in foil windings is of great importance in the design process of transformers, since, as it is well known, the current has a nonhomogeneous distribution along the cross section of the foil, which plays a significant role in the associated losses and also in the winding hot spot [1].

In the discipline of computational electromagnetics, there are essentially two main tendencies for solving practical engineering problems: 1) techniques based on analytical methods and 2) techniques based on numerical methods [2].

Techniques based on analytical methods were of primary importance when computing resources were very limited, and they are characterized by a short calculation time, which is achieved in most cases at the expense of applying strong simplifying assumptions.

In addition, techniques based on numerical methods have the advantage of providing greater flexibility to model complex geometries, and material anisotropies and nonlinearities. However, numerical methods are significantly slower and demanding in computational resources compared with methods based on analytical solutions. The most successful and widespread numerical technique in the technical and scientific environment is undoubtedly the finite-element method (FEM) [3].

Analytical techniques are still used today, even in low-frequency problems as presented in [4] and [5]. On the other hand, despite the great advances in numerical techniques in recent years, significant efforts are still being made to increase its efficiency and scope [6].

Mullineux *et al.* [7], El-Missiry [8], Ferreira [9], and Zúbek [10] have used analytical solutions to determine the current distribution and losses in foil windings; however, as already mentioned, these methods are based on simplified models, which are not usually sufficiently accurate and flexible for transformer design purposes.

To remedy the shortcomings of analytical models, solutions based on numerical methods to solve the problem of current distribution in foil windings have been proposed. Among these proposals are the works by Ram [1] and, recently, by Villén *et al.* [11], both using FEM.

The solution of the current distribution in foil windings using FEM presents additional challenges with respect to modeling windings made of traditional conductors. As it is known, the thickness of a foil turn is very small (from 0.5 to 3 mm thick), while its axial dimension is quite large and it can exceed 1 m height. This fact has the following implications.

1) Because the axial dimension is several times larger than the skin depth of the magnetic field δ, it is not feasible to solve the problem using a magnetostatic approach, making it necessary to perform a low-frequency harmonic simulation, which is more complex and requires more computation time than the magnetostatic solution [1].
2) To apply FEM, the whole problem region is to be discretized, including the space inside the conductors. As the thickness is so small and the axial dimension so large, the number of necessary elements to discretize all winding turns may become excessive, which drastically increases the simulation time.

The main objective of this paper is to propose a more flexible methodology than analytical methods and also much faster than the FEM, which is shown schematically in Fig. 1. Unlike FEM, the proposed method is based on integral equations, making it possible to perform the discretization of the problem only at the boundaries where material changes, which drastically reduces the size and computation time.

The general strategy presented in this paper is to replace the massive elements such as the core and foil conductors of the transformer by equivalent models represented by magnetic field sources controlled by boundary conditions.

Manuscript received November 12, 2014; revised March 24, 2015; accepted May 26, 2015. Date of publication June 2, 2015; date of current version August 17, 2015. Corresponding author: G. Diaz (e-mail: guandiaz@unisalle.edu.co).

Color versions of one or more of the figures in this paper are available online at http://ieeexplore.ieee.org.

Digital Object Identifier 10.1109/TMAG.2015.2440360

0018-9464 © 2015 IEEE. Personal use is permitted, but republication/redistribution requires IEEE permission.
See http://www.ieee.org/publications_standards/publications/rights/index.html for more information.

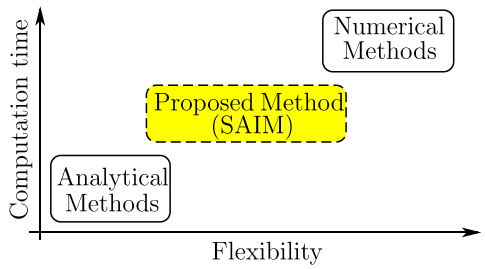

Fig. 1. Calculation methods.

II. Proposed Model

A. Equivalent Magnetic Model of the Transformer

As it is known, the transformer is a device consisting of an active part and a nonactive part, both having an inherently 3-D geometry. The active part is mainly composed of the core and windings (see Fig. 4), while elements such as the tank, frames, and shields form the nonactive part.

Although there exist magnetic phenomena in the elements of the nonactive part due to the stray flux of the windings and high currents flowing through the connections, the most important phenomena in the transformer occur in the active part.

In addition, although the transformer is a 3-D device, it has been shown that 2-D calculations are able to provide sufficiently reliable results for the determination of parameters such as current distribution, power losses, and Lorentz forces in the windings [12].

According to the above, this paper will focus on modeling the active part (core and windings) using an axisymmetric representation.

Although the active part is composed of massive elements such as the core and conductors, this paper has proposed an equivalent model where these massive elements are replaced by surface current distributions. For the case of surface currents representing the iron core, equivalent boundary conditions based on Ampere's law are fulfilled. In the case of the foil winding, the approach is to meet Faraday's law assuming low-frequency harmonic fields.

It has been assumed that the high-voltage winding is made of traditional conductors [paper-insulated rectangular wire (PIRW), magnet wire, etc.], so it has been modeled as a known surface current distribution. In the specific example analyzed, the high-voltage winding is a layer winding, wherein each layer has been represented by a cylindrical surface current distribution. For the case of disc coils, which are very common in high-voltage windings, the proposed model can be easily modified considering equivalent disk surface current distribution instead of cylindrical ones.

B. Equivalent Magnetic Model of the Core

Consider the boundary layout presented in Fig. 2(a), which will be called *the original arrangement*. The region ② in gray color represents the iron core material with permeability μ_2, while the yellow region ① represents the oil/air having magnetic permeability μ_0. It is assumed that the conductors

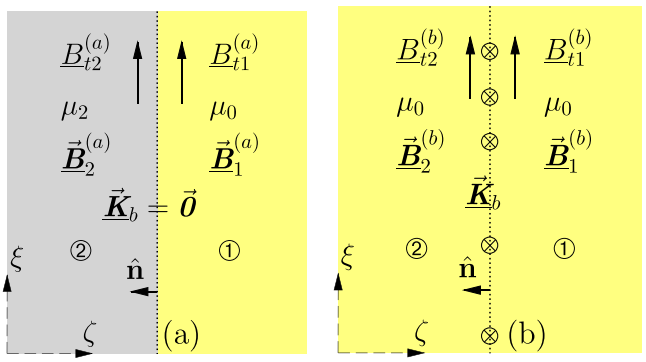

Fig. 2. (a) Original arrangement with magnetic material. (b) Equivalent arrangement without magnetic material.

are in region ① and that the permeability of the core is much higher than that of air, i.e., $\mu_2 \gg \mu_0$. In addition, it is assumed that no surface current is present at the boundary, i.e., $\underline{\vec{K}}_b = \vec{0}$. Note that the magnetic flux densities on each side of the boundary have the superscript (a), indicating the correspondence to *the original arrangement*.

Applying Ampere's law to *the original arrangement*, the following relationship between the tangential components of the magnetic flux density is found:

$$\hat{\mathbf{n}} \times \left(\underline{\vec{B}}_2^{(a)} \frac{1}{\mu_2} - \underline{\vec{B}}_1^{(a)} \frac{1}{\mu_0} \right) = \vec{0}. \tag{1}$$

Consider now *the equivalent arrangement* of Fig. 2(b). In this arrangement, the magnetic material has been removed and replaced by a material with magnetic permeability μ_0. In addition, a surface current distribution has been included $\underline{\vec{K}}_b \neq \vec{0}$ having a direction entering the picture plane. Note that the positive direction of the sheet current density is given by the direction of the unit vector $\hat{\boldsymbol{\nu}} = \hat{\boldsymbol{\xi}} \times \hat{\boldsymbol{\zeta}}$, where $\hat{\boldsymbol{\xi}}$ and $\hat{\boldsymbol{\zeta}}$ are the unit vectors in the directions of the axes ξ and ζ, respectively. Therefore, $\underline{\vec{K}}_b = \underline{K}_b \hat{\boldsymbol{\nu}}$.

The application of Ampere's law to this last case yields

$$\hat{\mathbf{n}} \times \left(\underline{\vec{B}}_2^{(b)} \frac{1}{\mu_0} - \underline{\vec{B}}_1^{(b)} \frac{1}{\mu_0} \right) = \underline{\vec{K}}_b. \tag{2}$$

Because the aim is that the equivalent arrangement reproduces the magnetic flux density distribution in media ① and ②, the following equation must hold:

$$\underline{\vec{B}}_1 := \underline{\vec{B}}_1^{(b)} = \underline{\vec{B}}_1^{(a)}, \quad \underline{\vec{B}}_2 := \underline{\vec{B}}_2^{(b)} = \underline{\vec{B}}_2^{(a)}. \tag{3}$$

Combining (1) and (2) with (3) and solving for the tangential components

$$\hat{\mathbf{n}} \times \underline{\vec{B}}_1 = \underline{\vec{K}}_b \frac{\mu_0^2}{\mu_2 - \mu_0} \tag{4}$$

$$\hat{\mathbf{n}} \times \underline{\vec{B}}_2 = \underline{\vec{K}}_b \frac{\mu_0 \mu_2}{\mu_2 - \mu_0}. \tag{5}$$

Because the magnetic permeability is μ_0 for both media ① and ② in the equivalent arrangement, the following relationships are valid:

$$\underline{\vec{B}}_1 = \mu_0 \underline{\vec{H}}_1^{(b)}, \quad \underline{\vec{B}}_2 = \mu_0 \underline{\vec{H}}_2^{(b)} \tag{6}$$

and since $\vec{\underline{H}}_1 := \vec{\underline{H}}_1^{(b)}$ and $\vec{\underline{H}}_2 := \vec{\underline{H}}_2^{(b)}$, (4) and (5) can be rewritten as follows:

$$\hat{\mathbf{n}} \times \vec{\underline{H}}_1 = \vec{\underline{K}}_b \frac{\mu_0}{\mu_2 - \mu_0} \tag{7}$$

$$\hat{\mathbf{n}} \times \vec{\underline{H}}_2 = \vec{\underline{K}}_b \frac{\mu_2}{\mu_2 - \mu_0}. \tag{8}$$

The surface current density $\vec{\underline{K}}_b$ on the boundary causes a discontinuity in the magnetic field intensity on both sides of the boundary, which satisfies the following relationship:

$$\hat{\mathbf{n}} \times \vec{\underline{H}}_b = \hat{\mathbf{n}} \times \left(\frac{\vec{\underline{H}}_1 + \vec{\underline{H}}_2}{2} \right) \tag{9}$$

where $\hat{\mathbf{n}} \times \vec{\underline{H}}_b$ is the tangential magnetic field intensity on the boundary. Substituting (7) and (8) in (9), the following equation is obtained:

$$\hat{\mathbf{n}} \times \vec{\underline{H}}_b = \frac{1}{2} \left(\frac{\mu_{r2} + 1}{\mu_{r2} - 1} \right) \vec{\underline{K}}_b \tag{10}$$

where $\mu_{r2} = \mu_2/\mu_0$ is the relative permeability of the core. Defining $\kappa_m = (1/2)(\mu_{r2} + 1)/(\mu_{r2} - 1)$ as the magnetic intrinsic property of the core material, (10) can be simply written as

$$\hat{\mathbf{n}} \times \vec{\underline{H}}_b = \kappa_m \vec{\underline{K}}_b. \tag{11}$$

Equation (11) is very important since it relates the value of the tangential magnetic field intensity with the surface current density, both present on the boundary between the two media. Therefore, if the surface current density distribution on the boundary satisfies (11), the magnetic flux densities in the equivalent arrangement will be exactly the same as in the original arrangement. Because of this, (11) will be referred to as the *core boundary equation*.

Defining $\hat{\mathbf{n}} \times \vec{\underline{H}}_b = \underline{H}_t \hat{\mathbf{v}}$, where $\underline{H}_t$ is the scalar component of the tangential field intensity on the boundary, the scalar version of the core boundary equation can be written as follows:

$$\underline{H}_t = \kappa_m \underline{K}_b. \tag{12}$$

The advantage of the *equivalent arrangement* with respect to the *original arrangement* is that if a traditional method such as FEM is applied to the *original arrangement*, both media ① and ② must be completely discretized regardless of the location of the actual points of interest, whereas for the *equivalent arrangement*, only the boundary between the two media is to be discretized, which implies a drastic reduction in the size and complexity of the problem in comparison with the *original arrangement*.

C. Equivalent Magnetic Model of a Foil Turn

Let us consider the foil turn segment of thickness d and conductivity σ shown in Fig. 3(a). As it can be seen, the conductor has a current density $\vec{\underline{J}}(r, z)$. This current density can be decomposed into two components $\vec{\underline{J}} = \vec{\underline{J}}_{\text{src}} + \vec{\underline{J}}_{\text{eddy}}$, where $\vec{\underline{J}}_{\text{eddy}} = -\text{j}\omega\sigma\vec{\underline{A}}$ and $\vec{\underline{J}}_{\text{src}} = -\sigma\nabla\underline{V}$. Because the thickness of the foil turn d is much less than the magnetic field skin depth δ, the thin-sheet[1] approximation is valid [13]

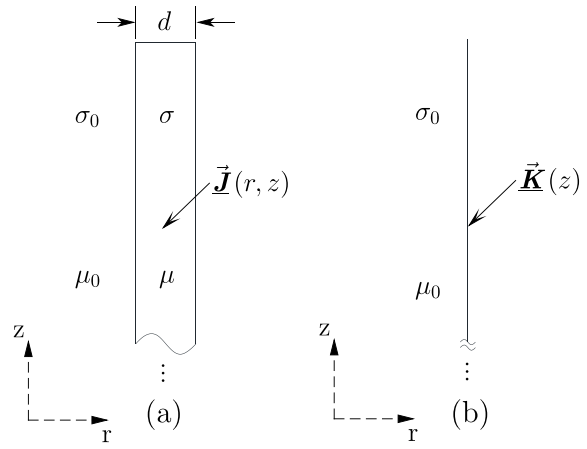

Fig. 3. (a) Original arrangement of a foil conductor. (b) Equivalent arrangement of a foil conductor.

$$\vec{\underline{J}}_{\text{eddy}} = \frac{1}{d} \vec{\underline{K}}_{\text{eddy}}. \tag{13}$$

From (13), the following expression for the surface current density can be derived:

$$\vec{\underline{K}}_{\text{eddy}} = -\text{j}d\omega\sigma\vec{\underline{A}}. \tag{14}$$

Defining $\underline{\kappa}_l = -\text{j}d\omega\sigma$ as a constant, which depends on the material properties of the foil conductor, $\vec{\underline{K}}_{\text{eddy}} = \underline{\kappa}_l \vec{\underline{A}}$ is obtained, or in scalar form

$$\underline{K}_{\text{eddy}} = \underline{\kappa}_l \underline{A}_\phi. \tag{15}$$

Note that the component in the azimuthal direction $\underline{A}_\phi$ has been considered since the problem is axisymmetric. Also note that the surface current density can be expressed as the superposition of the eddy current component and the component due to the electric potential as follows:

$$\vec{\underline{K}} = \vec{\underline{K}}_{\text{src}} + \vec{\underline{K}}_{\text{eddy}}. \tag{16}$$

Equation (15) is called the *foil conductor boundary equation*, because if a current density distribution $\vec{\underline{J}}$ is replaced by a surface current density $\vec{\underline{K}}$ that satisfies (15), it is to be assumed that both arrangements are magnetically equivalent. The original and equivalent arrangements are shown in Fig. 3(a) and (b), respectively.

D. Equivalent Magnetic Model of Traditional Conductors

It has been assumed in this paper that the high-voltage winding is built using traditional conductors like PIRW.

Because the dimensions of the conductors are not considerably larger than δ, the current distribution in these windings is readily predictable and therefore can be assumed to be known.

The most important point to bear in mind is that the total magnetomotive force of this winding must be equal to that of the low-voltage winding and having opposite sign,

[1]For a detailed exposition of the thin sheet approximation, see [13, Sec. 4.4].

which is a consequence of Faraday's law. The magnitudes of the magnetomotive forces of both windings are not actually the same due to the no-load current; however, this effect can be ignored without causing significant errors in the results.

In addition, a high-voltage layer winding has been considered, where each layer has been represented by a cylinder of infinitesimal thickness having a surface current density that is constant along its axial dimension. The value of the current density of each cylinder is calculated as the total number of turns of the layer multiplied by the phase current divided by the axial dimension of the cylinder. The axial dimension of each cylinder corresponds to the magnetic height of the corresponding layer.

III. Solution Methodology

A. Unknowns and Known Model Information

The boundary conditions to model the foil winding and iron core have been given in Sections II-B and II-C. As it can be seen, the two boundary conditions of (12) and (15) have been expressed in terms of the surface current, so it is necessary to define the mathematical expressions of the magnetic field produced by surface current densities. Due to the particular geometry of the transformer, its geometry can be represented using cylindrical and disk-shaped elements. The mathematical expressions for the magnetic field produced by these two model elements are available in [14] and [15].

The characteristic of the expressions presented in [14] and [15] is that the surface current density has been considered to have a linear variation over the axial dimension of the element, which allows one to model large areas of surface current density avoiding current discontinuities, improving in this way the quality and accuracy of the results. In general, the magnetic vector potential, the radial magnetic field intensity, and the axial magnetic field intensity produced by an element i on a field point j are denoted, respectively, as follows:

$$\underline{A}_{\phi}^{[j,i]} = \frac{\mu_0}{2\pi}\int_{p_1}^{p_2}\int_{0}^{\pi}\underline{J}^{[j,i]}\mathrm{d}\phi'\mathrm{d}l' = k_{\phi 1}^{[j,i]}\underline{K}_{\phi 1}^{[i]} + k_{\phi 2}^{[j,i]}\underline{K}_{\phi 2}^{[i]} \quad (17)$$

$$\underline{H}_{r}^{[j,i]} = -\frac{1}{2\pi}\int_{p_1}^{p_2}\int_{0}^{\pi}\frac{\partial \underline{J}^{[j,i]}}{\partial z}\mathrm{d}\phi'\mathrm{d}l' = k_{r1}^{[j,i]}\underline{K}_{\phi 1}^{[i]} + k_{r2}^{[j,i]}\underline{K}_{\phi 2}^{[i]} \quad (18)$$

$$\underline{H}_{z}^{[j,i]} = \frac{1}{2\pi r}\int_{p_1}^{p_2}\int_{0}^{\pi}\frac{\partial (r\cdot \underline{J}^{[j,i]})}{\partial r}\mathrm{d}\phi'\mathrm{d}l' = k_{z1}^{[j,i]}\underline{K}_{\phi 1}^{[i]} + k_{z2}^{[j,i]}\underline{K}_{\phi 2}^{[i]} \quad (19)$$

where $k_{\phi 1}^{[j,i]}$, $k_{\phi 2}^{[j,i]}$, $k_{r1}^{[j,i]}$, $k_{r2}^{[j,i]}$, and $k_{z1}^{[j,i]}$ y $k_{z2}^{[j,i]}$ are real numbers that are only a function of the element geometry and field point coordinates, for which these will be referred to as *geometry-dependent factors* throughout this paper.

The solution of the integral (17)–(19) is presented in detail in [14] and [15].

Note that the current densities $\underline{K}_{\phi 1}^{[i]}$ and $\underline{K}_{\phi 2}^{[i]}$ may or may not be known depending on the part of the transformer being modeled. In Fig. 4, a 3-D model of the transformer active part is presented. As can be observed, a 2-D cut has been included highlighting the sections of the high-voltage winding, low-voltage winding, and also the boundary between the oil/air and the core. In Fig. 5, the detail of the axisymmetric model of the core is presented, which is composed of an arrangement of cylinders and disks located on the boundary between media ① and ②. The low-voltage foil winding is shown in blue, while the high-voltage winding is shown in green.

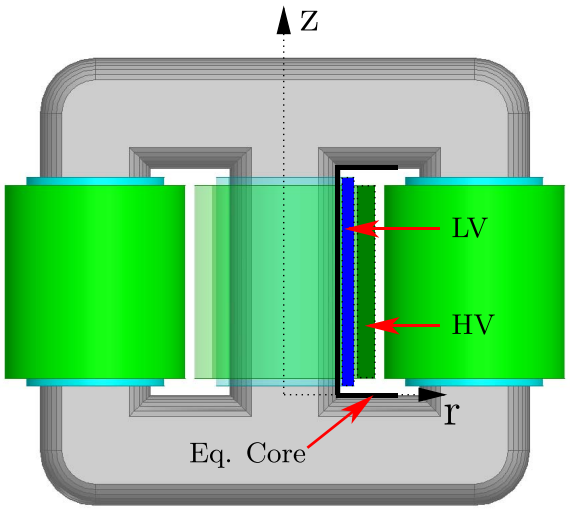

Fig. 4. 3-D model of the transformer active part.

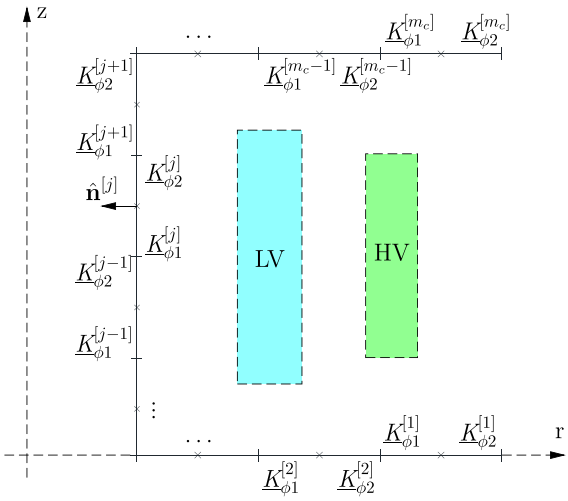

Fig. 5. General transformer model layout.

As observed in Fig. 5, each element has two characteristic values of surface current density. Each element is identified by the element number in brackets as superscript. In addition, each element belonging to the core has an associated evaluation point in its central part, which is represented in Fig. 5 by an x.

The total number of elements of the problem is n, from which m elements have an unknown current density. From these m elements with unknown current density, m_c belong to the core and m_f to the foil winding.

B. Iron Core Equations

According to the above, the tangential field strength produced by the element i on the field point of the element j

belonging to the core can be expressed as

$$\underline{H}_t^{[j,i]} = k_{t1}^{[j,i]}\underline{K}_{\phi 1}^{[i]} + k_{t2}^{[j,i]}\underline{K}_{\phi 2}^{[i]} \quad \text{for} \quad i = 1,\ldots,n,\ j = 1,\ldots,m_c. \tag{20}$$

Note that the factors $k_{t1}^{[j,i]}$ and $k_{t2}^{[j,i]}$ may be related to the radial or axial field depending on the location of the jth element. For example, the elements belonging to the core leg are related to the axial component, while the elements of the yokes are related to the radial component of the field.

The tangential field intensity on the field point of element j is the superposition of the contributions of all elements including the contribution of the element itself, which can be written as follows:

$$\underline{H}_t^{[j]} = \sum_{i=1}^{n} \underline{H}_t^{[j,i]} = \underline{H}_t^{[j,j]} + \sum_{\substack{i=1 \\ i\neq j}}^{m_c} \underline{H}_t^{[j,i]} + \sum_{i=m_c+1}^{m} \underline{H}_t^{[j,i]} + \sum_{i=m+1}^{n} \underline{H}_t^{[j,i]} \tag{21}$$

for $j = 1,\ldots,m_c$. In (21), the contributions from the core and the low-voltage winding and high-voltage winding have been separated. In the case of the high-voltage winding, it is assumed that the distribution of magnetomotive force is known and, therefore, the surface current density as well. By substituting (20) in (21), the following expression is obtained:

$$\begin{aligned}\underline{H}_t^{[j]} = {} & k_{t1}^{[j,j]}\underline{K}_{\phi 1}^{[j]} + k_{t2}^{[j,j]}\underline{K}_{\phi 2}^{[j]} + \sum_{\substack{i=1 \\ i\neq j}}^{m_c}\left(k_{t1}^{[j,i]}\underline{K}_{\phi 1}^{[i]} + k_{t2}^{[j,i]}\underline{K}_{\phi 2}^{[i]}\right) \\ & + \sum_{i=m_c+1}^{m}\left(k_{t1}^{[j,i]}\underline{K}_{\phi 1}^{[i]} + k_{t2}^{[j,i]}\underline{K}_{\phi 2}^{[i]}\right) \\ & + \sum_{i=m+1}^{n}\left(k_{t1}^{[j,i]}\underline{K}_{\phi 1}^{[i]} + k_{t2}^{[j,i]}\underline{K}_{\phi 2}^{[i]}\right).\end{aligned} \tag{22}$$

According to what was stated in Section II-B, the following boundary condition must be satisfied in each iron core element:

$$\underline{H}_t^{[j]} = \kappa_m \underline{K}_b^{[j]} \nu^{[j]}. \tag{23}$$

Unlike (12), the variable $\nu^{[j]}$ has been added to apply the correct sign to the boundary condition according to the direction of the element normal vector relative to the global coordinate system (r–z). It should be noted that each element in the core has a local coordinate system for which the relationship $\hat{\boldsymbol{\nu}}^{[j]} = \hat{\boldsymbol{\xi}}^{[j]} \times \hat{\boldsymbol{\zeta}}^{[j]}$ holds, so it can be defined as

$$\nu^{[j]} = \begin{cases} -1 & \text{when } \hat{\boldsymbol{\nu}}^{[j]} = -\hat{\boldsymbol{\phi}} \\ 1 & \text{when } \hat{\boldsymbol{\nu}}^{[j]} = \hat{\boldsymbol{\phi}}. \end{cases} \tag{24}$$

Equation (24) can be written in a more simple form as

$$\nu^{[j]} = \begin{cases} -1 & \text{for} \quad j = 1,\ldots,m_{\text{yc}} \\ 1 & \text{for} \quad m_{\text{yc}}+1,\ldots,m_c \end{cases} \tag{25}$$

where m_{yc} is the number of elements that make up each yoke, assuming that both the lower and the upper yoke have the same number of elements. Recalling that elements having linear current density are being used, it can be easily shown that the current density at the center of the element is simply the average of the values of its ending edges

$$\underline{K}_b^{[j]} = \frac{\underline{K}_{\phi 1}^{[j]} + \underline{K}_{\phi 2}^{[j]}}{2}. \tag{26}$$

Note that the variable $\underline{K}_b^{[j]}$ has been used for the current density at the center of the element, because the field points are located exactly at this place, and therefore, there is where the boundary condition is to be evaluated. According to the above, substituting (26) in (23), it can be written as

$$\underline{H}_t^{[j]} = \frac{\kappa_m}{2}\nu^{[j]}\left(\underline{K}_{\phi 1}^{[j]} + \underline{K}_{\phi 2}^{[j]}\right). \tag{27}$$

The substitution of (27) into (22) and a subsequent rearrangement gives

$$\begin{aligned}&\left(\frac{\kappa_m}{2}\nu^{[j]} - k_{t1}^{[j,j]}\right)\underline{K}_{\phi 1}^{[j]} + \left(\frac{\kappa_m}{2}\nu^{[j]} - k_{t2}^{[j,j]}\right)\underline{K}_{\phi 2}^{[j]} \\ &\quad - \sum_{\substack{i=1 \\ i\neq j}}^{m_c}\left(k_{t1}^{[j,i]}\underline{K}_{\phi 1}^{[i]} + k_{t2}^{[j,i]}\underline{K}_{\phi 2}^{[i]}\right) \\ &\quad - \sum_{i=m_c+1}^{m}\left(k_{t1}^{[j,i]}\underline{K}_{\phi 1}^{[i]} + k_{t2}^{[j,i]}\underline{K}_{\phi 2}^{[i]}\right) \\ &= \sum_{i=m+1}^{n}\left(k_{t1}^{[j,i]}\underline{K}_{\phi 1}^{[i]} + k_{t2}^{[j,i]}\underline{K}_{\phi 2}^{[i]}\right) \\ &\qquad\qquad \text{for } j = 1,\ldots,m_c.\end{aligned} \tag{28}$$

Note that (28) represents a set of m_c equations with $2m_c$ unknowns.

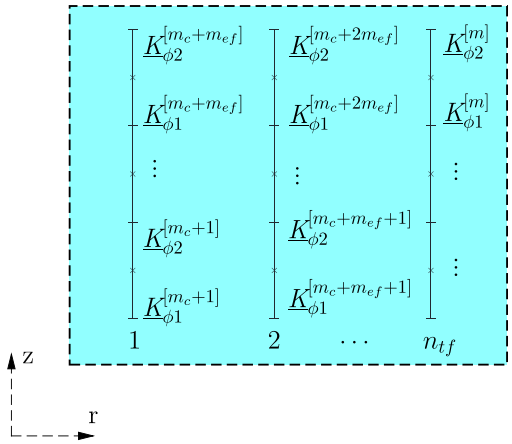

Fig. 6. Low-voltage winding elements represented using surface current elements.

C. Foil Winding Equations

Let us consider Fig. 6. This shows the equivalent model of a coil of n_{tf} turns of a foil winding, where each one has been represented by an arrangement of m_{ef} cylindrical elements. In this paper, it is assumed that the number of elements m_{ef} modeling a foil turn is odd. Similar to the iron core elements, it has been provided a field point at the center of each element.

The magnetic vector potential contribution of the element i at the field point of element j is given by

$$\underline{A}_{\phi}^{[j,i]} = k_{\phi 1}^{[j,i]} \underline{K}_{\phi 1}^{[i]} + k_{\phi 2}^{[j,i]} \underline{K}_{\phi 2}^{[i]} \tag{29}$$

for $i = 1, \ldots, n$ and $j = m_c+1, \ldots, m$. Note that a field point has been placed in the central part of each element belonging to the foil winding. Furthermore, the magnetic vector potential at point j can be written as

$$\underline{A}_{\phi}^{[j]} = \sum_{i=1}^{m_c} \underline{A}_{\phi}^{[j,i]} + \underline{A}_{\phi}^{[j,j]} + \sum_{\substack{i=m_c+1 \\ i \neq j}}^{m} \underline{A}_{\phi}^{[j,i]} + \sum_{i=m+1}^{n} \underline{A}_{\phi}^{[j,i]}. \tag{30}$$

By substituting (29) in (30), the following equation is obtained:

$$\begin{aligned} \underline{A}_{\phi}^{[j]} = & \sum_{i=1}^{m_c} \left(k_{\phi 1}^{[j,i]} \underline{K}_{\phi 1}^{[i]} + k_{\phi 2}^{[j,i]} \underline{K}_{\phi 2}^{[i]} \right) + k_{\phi 1}^{[j,j]} \underline{K}_{\phi 1}^{[j]} + k_{\phi 2}^{[j,j]} \underline{K}_{\phi 2}^{[j]} \\ & + \sum_{\substack{i=m_c+1 \\ i \neq j}}^{m} \left(k_{\phi 1}^{[j,i]} \underline{K}_{\phi 1}^{[i]} + k_{\phi 2}^{[j,i]} \underline{K}_{\phi 2}^{[i]} \right) \\ & + \sum_{i=m+1}^{n} \left(k_{\phi 1}^{[j,i]} \underline{K}_{\phi 1}^{[i]} + k_{\phi 2}^{[j,i]} \underline{K}_{\phi 2}^{[i]} \right). \end{aligned} \tag{31}$$

Furthermore, according to the foil conductor boundary (15), the following equation must be satisfied for the jth element:

$$\underline{K}_{\text{eddy}}^{[j]} = \underline{\kappa}_l \underline{A}_{\phi}^{[j]}. \tag{32}$$

According to (16), it can also be written as

$$\underline{K}_{b}^{[j]} = \underline{K}_{\text{eddy}}^{[j]} + \underline{K}_{\text{src}}^{[j]} \tag{33}$$

where $\underline{K}_{b}^{[j]}$ represents the surface current density at the center of element j. Substituting (32) and (26) in (33) and rearranging it is obtained that

$$\underline{K}_{\phi 1}^{[j]} + \underline{K}_{\phi 2}^{[j]} - 2\underline{\kappa}_l \underline{A}_{\phi}^{[j]} - 2\underline{K}_{\text{src}}^{[j]} = 0. \tag{34}$$

Substituting (31) in (34), after some algebraic manipulations, the following equation is obtained:

$$\begin{aligned} & -2\underline{\kappa}_l \sum_{i=1}^{m_c} \left(k_{\phi 1}^{[j,i]} \underline{K}_{\phi 1}^{[i]} + k_{\phi 2}^{[j,i]} \underline{K}_{\phi 2}^{[i]} \right) + \left(1 - 2\underline{\kappa}_l k_{\phi 1}^{[j,j]} \right) \underline{K}_{\phi 1}^{[j]} \\ & + \left(1 - 2\underline{\kappa}_l k_{\phi 2}^{[j,j]} \right) \underline{K}_{\phi 2}^{[j]} - 2\underline{\kappa}_l \sum_{\substack{i=m_c+1 \\ i \neq j}}^{m} \left(k_{\phi 1}^{[j,i]} \underline{K}_{\phi 1}^{[i]} + k_{\phi 2}^{[j,i]} \underline{K}_{\phi 2}^{[i]} \right) \\ & - 2\underline{K}_{\text{src}}^{[j]} = 2\underline{\kappa}_l \sum_{i=m+1}^{n} \left(k_{\phi 1}^{[j,i]} \underline{K}_{\phi 1}^{[i]} + k_{\phi 2}^{[j,i]} \underline{K}_{\phi 2}^{[i]} \right) \\ & \text{for } j = m_c + 1, \ldots, m. \end{aligned} \tag{35}$$

Note that (35) represents a set of m_f equations. It should be noted that the surface current densities $\underline{K}_{\text{src}}^{[j]}$ are also unknown so that the number of unknowns in (35) is $3m_f$. It should be noted that the component of the surface current density associated to the electric potential source is constant for a given radius, and therefore, advantage of this fact will be taken to reduce the number of unknowns, creating the new variable $\underline{K}_{\text{src}}^{(\text{tr})[p]}$, which is

$$\underline{K}_{\text{src}}^{(\text{tr})[p]} = \underline{K}_{\text{src}}^{[j]} \quad \text{for } j = m_c + 1, \ldots, m \tag{36}$$

where $p = \lceil (j - m_c) / m_{\text{ef}} \rceil$ and consequently $p = 1, \ldots, m_{\text{ef}}$. The notation $\lceil x \rceil$ means the smallest integer greater than or equal to x. Accordingly, (36) can be rewriten as follows:

$$\begin{aligned} & -\sum_{i=1}^{m_c} \left(k_{\phi 1}^{[j,i]} \underline{K}_{\phi 1}^{[i]} + k_{\phi 2}^{[j,i]} \underline{K}_{\phi 2}^{[i]} \right) + \left(\frac{1}{2\underline{\kappa}_l} - k_{\phi 1}^{[j,j]} \right) \underline{K}_{\phi 1}^{[j]} \\ & + \left(\frac{1}{2\underline{\kappa}_l} - k_{\phi 2}^{[j,j]} \right) \underline{K}_{\phi 2}^{[j]} - \sum_{\substack{i=m_c+1 \\ i \neq j}}^{m} \left(k_{\phi 1}^{[j,i]} \underline{K}_{\phi 1}^{[i]} + k_{\phi 2}^{[j,i]} \underline{K}_{\phi 2}^{[i]} \right) \\ & - \frac{1}{\underline{\kappa}_l} \underline{K}_{\text{src}}^{(\text{tr})[p]} = \sum_{i=m+1}^{n} \left(k_{\phi 1}^{[j,i]} \underline{K}_{\phi 1}^{[i]} + k_{\phi 2}^{[j,i]} \underline{K}_{\phi 2}^{[i]} \right) \\ & \text{for } p = \lceil (j - m_c) / m_{\text{ef}} \rceil, \quad j = m_c + 1, \ldots, m. \end{aligned} \tag{37}$$

In a foil winding, each turn is in series with the next one, and additionally, the elements belonging to the same turn are at the same electrical potential, and therefore, the sum of the currents from each element of the turn must be equal to the phase current of the transformer $\underline{I}_{\phi}^{(f)}$. This can be written as follows:

$$\underline{I}_{\phi}^{(f)} = \frac{1}{2} \sum_{\substack{j=m_c+ \\ (p-1)m_{\text{ef}}+1}}^{m_c+p \cdot m_{\text{ef}}} h_e^{[j]} \left(\underline{K}_{\phi 1}^{[j]} + \underline{K}_{\phi 2}^{[j]} \right) \tag{38}$$

with $p = 1, \ldots, n_{\text{tf}}$ and where $h_e^{[j]}$ is the axial dimension (height) of the jth element.

D. Equations for Linking the Different Elements

A set of $m_c + m_f + n_{\text{tf}}$ equations with $2m_c + 2m_f + n_{\text{tf}}$ unknowns have been defined so far. To obtain the complete system of equations, it is necessary to set out additional equations. As shown in Figs. 5 and 6, there are points where the end of an element coincides with the beginning of another element, and at these points, the surface current densities must be the same. The following equation sets these conditions:

$$\begin{aligned} & \underline{K}_{\phi 1}^{[j]} - \underline{K}_{\phi 2}^{[j+1]} = 0 \quad \text{for } j = 1, \ldots, m_{\text{yc}} - 1 \\ & \underline{K}_{\phi 1}^{[j]} - \underline{K}_{\phi 1}^{[j+1]} = 0 \quad \text{for } j = m_{\text{yc}} \\ & \underline{K}_{\phi 2}^{[j]} - \underline{K}_{\phi 1}^{[j+1]} = 0 \quad \text{for } j = m_{\text{yc}} + 1, \ldots, m_c - 1 \\ & \underline{K}_{\phi 2}^{[1]} - \underline{K}_{\phi 2}^{[m_c]} = 0. \end{aligned} \tag{39}$$

Equation (39) has the purpose of linking the core elements. The following equation links the elements of the foil winding:

$$\begin{aligned} & \underline{K}_{\phi 2}^{[m_c+m_{\text{ef}}(p-1)+i]} - \underline{K}_{\phi 1}^{[m_c+m_{\text{ef}}(p-1)+i+1]} = 0 \\ & \qquad \text{for } i = 1, \ldots, m_{\text{ef}} - 1, \quad p = 1, \ldots, n_{\text{tf}} \end{aligned} \tag{40}$$

$$\begin{aligned} & \underline{K}_{\phi 1}^{\left[m_c+\frac{1}{2}(m_{\text{ef}}+1)+(p-1)m_{\text{ef}}\right]} - \underline{K}_{\phi 2}^{\left[m_c+\frac{1}{2}(m_{\text{ef}}+1)+(p-1)m_{\text{ef}}\right]} = 0 \\ & \qquad \text{for } p = 1, \ldots, n_{\text{tf}}. \end{aligned} \tag{41}$$

Note that in addition to the linking equations (40), additional equations (41) have been added to obtain a complete

system. These equations can be formulated from the fact that the current density at the center of the turns is fairly uniform, so it is possible to impose that the current density is constant at the central element without a significant loss of accuracy.

E. Equation System Formulation

From (28) and (37)–(41), it is relatively simple to pose a system of linear equations in matrix form. With this aim, the following matrix system is considered:

$$\underline{\mathbf{M}}_{\text{sys}} = \begin{bmatrix} \mathbf{k}_t^{(\text{cc})} + \mathbf{M}_b^{(c)} & \mathbf{k}_t^{(\text{fc})} & \mathbf{0} \\ \mathbf{k}_\phi^{(\text{cf})} & \mathbf{k}_\phi^{(\text{ff})} + \underline{\mathbf{M}}_b^{(f)} & \underline{\mathbf{M}}_{\text{src}}^{(f)} \\ \mathbf{0} & \mathbf{h}^{(f)} & \mathbf{0} \\ \mathbf{M}_v^{(c)} & \mathbf{0} & \mathbf{0} \\ \mathbf{0} & \mathbf{M}_v^{(f)} & \mathbf{0} \end{bmatrix}. \quad (42)$$

The system matrix $\underline{\mathbf{M}}_{\text{sys}}$ is a square matrix of dimension $2m + n_{\text{tf}}$ composed of the submatrices $\mathbf{k}_t^{(\text{cc})}$, $\mathbf{k}_t^{(\text{fc})}$, $\mathbf{k}_\phi^{(\text{cf})}$, and $\mathbf{k}_\phi^{(\text{ff})}$, which are called the core–core, foil–core, core–foil, and foil–foil interaction matrices, respectively. These matrices contain the geometry-dependent factors related to the interaction of a given element considered as a source and the field point of another element or of the element itself. Note that all elements of these matrices are known since they depend only on the geometry of the field source and the coordinate of the field point.

The matrices $\mathbf{M}_b^{(c)}$ and $\underline{\mathbf{M}}_b^{(f)}$ contain the boundary conditions related to the elements of the core and the foil winding, respectively. On the other hand, $\mathbf{M}_v^{(c)}$ and $\mathbf{M}_v^{(f)}$ are called the linkage matrices because they contain the information of the linking equations (39)–(41).

The matrix $\mathbf{h}^{(f)}$ contains the axial dimensions of the foil winding elements, while the matrix $\underline{\mathbf{M}}_{\text{src}}^{(f)}$ contains the factor $1/\underline{\kappa}_l$ that affects the current densities related to the electrical potential. Let us now consider the vectors with the known information $\underline{\mathbf{b}}_{\text{sys}}$ and the vector of the unknowns $\underline{\mathbf{x}}_{\text{sys}}$ as follows:

$$\underline{\mathbf{b}}_{\text{sys}} = \begin{bmatrix} \underline{\mathbf{H}}_t^{(\text{hc})} \\ \underline{\mathbf{A}}_\phi^{(\text{hf})} \\ 2\underline{I}_\phi^{(f)} \cdot \mathbf{1} \\ \mathbf{0} \end{bmatrix}, \quad \underline{\mathbf{x}}_{\text{sys}} = \begin{bmatrix} \underline{\mathbf{K}}_\phi^{(\text{uk})} \\ \underline{\mathbf{K}}_{\text{src}}^{(\text{uk})} \end{bmatrix}. \quad (43)$$

As it can be seen, the vector $\underline{\mathbf{b}}_{\text{sys}}$ contains, at the same time, the vector $\underline{\mathbf{H}}_t^{(\text{hc})}$ that corresponds to the tangential magnetic field strength produced by the elements of the high-voltage winding on the core. Similarly, the vector $\underline{\mathbf{A}}_\phi^{(\text{hf})}$ contains the contributions of the magnetic vector potential of the high-voltage winding on the elements of the foil winding. Furthermore, the matrix $\underline{\mathbf{K}}_\phi^{(\text{uk})}$ contains the surface current densities of the iron core and of the foil winding, while the matrix $\underline{\mathbf{K}}_{\text{src}}^{(\text{uk})}$ contains the surface current densities related to the electric potential source of the foil winding.

According to the above, the values of the surface current densities of the iron core and of the foil winding can be determined by solving the following system of linear equations:

$$\underline{\mathbf{M}}_{\text{sys}} \cdot \underline{\mathbf{x}}_{\text{sys}} = \underline{\mathbf{b}}_{\text{sys}}. \quad (44)$$

TABLE I
GENERAL PARAMETERS OF THE REFERENCE TRANSFORMER

Parameter	Value
General information	
Rated Power	10 MVA
Vector Group	Dyn11
Rated Frequency	60 Hz
Primary Rated Voltage	13 800 Vrms
Primary Rated Current (Line)	418.37 Arms
Secondary Rated Voltage (Line-Line)	2 400 Vrms
Secondary Rated Current (Line)	2 405.63 Arms
Low Voltage Winding	
Construction Type	Foil
Conductor Material	Copper
Radial Bare Conductor Width	0.9 mm
Axial Bare Conductor Height	762 mm
Winding Width	45 mm
Distance to Lower Yoke	25 mm
Distance to Upper Yoke	40 mm
Number of Turns	26
High voltage winding	
Construction Type	Layer
Conductor Material	Copper
Axial winding height	732 mm
Radial winding width	64 mm
Distance to Lower Yoke	40 mm
Distance to Upper Yoke	55 mm
Number of Layers	10
Iron Core	
Construction Type	Core Type
Window Height	827 mm
Window Width	291 mm
Leg Diameter	403 mm

Equation (44) is a complex system of linear equations that can be solved very efficiently by the lower–upper decomposition method.

IV. VALIDATION OF THE PROPOSED METHODOLOGY

To compare the computation time and accuracy of the proposed methodology, a real transformer with low-voltage foil winding has been modeled. The transformer model is axisymmetric and it has been calculated using FEM and the proposed methodology semianalytic integral method (SAIM).

A. Description of the Case Study

The case study is a 10 MVA transformer with a low-voltage foil winding that is divided into four sections separated by cooling ducts. The high-voltage winding is a layer winding made of rectangular conductors. Table I shows the most important information of the transformer.

B. Results Using FEM

To simulate the transformer in the case study, the FEM program magnet (Infolytica) has been used on a 2.8 MHz Core i7, 8 GB RAM computer. The transformer was simulated at a frequency of 60 Hz and the foil turns of the winding have been modeled in detail. The high-voltage winding has been represented in simplified form by cylinders, representing each layer of the winding.

The most important attributes of the FEM simulation are presented in the second column of Table III. In Fig. 7,

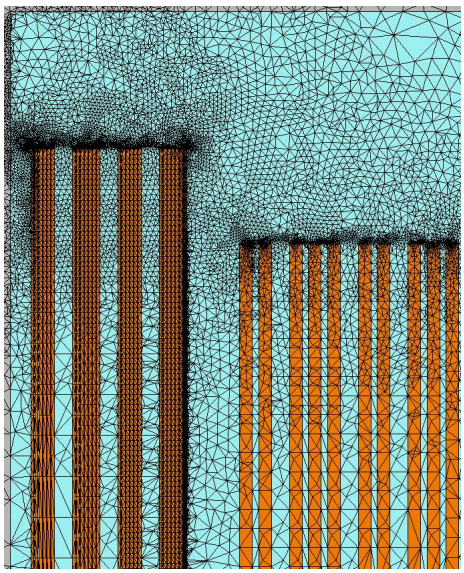

Fig. 7. Final mesh at the top of the window generated by Infolytica Magnet.

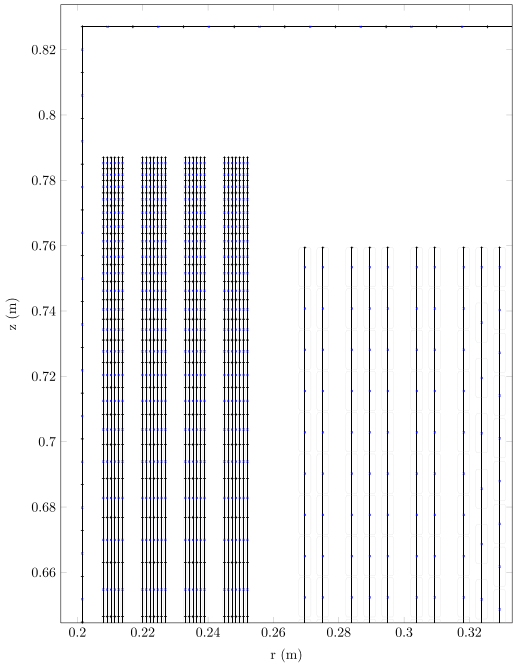

Fig. 8. Discretization of the upper part of the core window.

the final mesh of the upper part of the transformer of the case study is presented. Magnet uses an adaptive meshing scheme that uses more elements in regions with higher field variations. In this case, a large number of elements is shown in the upper part of windings since the field at these points has a fairly sharp increase in the radial magnetic field component.

C. Results Using SAIM

Fig. 8 shows an equivalent representation of the upper part of the analyzed transformer using SAIM. A number of $m_{\mathrm{lc}} = 59$ elements have been used for modeling the core leg and $m_{\mathrm{yc}} = 13$ elements for each yoke. Consequently, the core has been modeled using $m_c = m_{\mathrm{lc}} + 2m_{\mathrm{yc}} = 85$ elements.

TABLE II
SUMMARY OF THE TOTAL POWER LOSSES OF THE WINDINGS

Method	$P^{(f)}$(W)	$P^{(h)}$(W)
FEM	6 118.2	7 083.7
SAIM	6 141.0	7 172.1

For the foil winding, each turn has been represented with a set of $m_{\mathrm{ef}} = 49$ elements, so all the winding needed $m_{\mathrm{ef}} \cdot n_{\mathrm{tf}} = 1274$ elements. As observed in Fig. 8, the distribution of elements is not uniform so that most elements are concentrated at the coil ends where the highest variations of the current density arise.

For the modeling of the high-voltage winding, 11 cylinders have been used, one for each layer. Two cylinders have been used in the outermost layer to model the effect of magnetic gap caused by the tap changer in the rated voltage tap. According to the above, the transformer model needed $n = 85 + 1274 + 11 = 1370$ elements. From these elements, only those in the high-voltage winding have known surface current densities, while $m = 1359$ elements have unknown surface current densities, which are determined from the solution of the system of linear equations(44).

Once the system of linear equations has been solved, it is possible to determine the value of the foil winding losses from the surface current densities using (45). In the following, v' is the volume of the foil turn segment on which the losses are being calculated:

$$P = \frac{1}{2\sigma d^2} \int_{\mathrm{v}'} \underline{\vec{\boldsymbol{K}}} \cdot \underline{\vec{\boldsymbol{K}}}^{*} dv'. \tag{45}$$

The sum of the losses of all segments of all turns leads to the total loss value in the foil winding $P^{(f)}$, which is reported in Table II.

The magnetic flux density at the positions of each conductor of the high-voltage winding can be determined from the surface current density values of the equivalent models of the iron core, the foil winding, and the high-voltage winding. The value of the additional losses due to eddy currents, whose formulations are presented in [16] and [17], can be calculated from these flux density values and the turn dimensions. The sum of the resistive and additional losses of each turn of the high-voltage winding is the total loss of the winding $P^{(h)}$, which is presented in Table II.

D. Comparison of Results Obtained With FEM and SAIM

Table II summarizes the low- and high-voltage winding losses calculated with FEM and SAIM. The results are quite similar to differences lower than 2%.

On the other hand, Table III presents a comparison of the computational performances of FEM and SAIM. As it can be seen, FEM required about 80 times more elements than SAIM. The number of degrees of freedom refers to the number of unknowns of the problem, which in the case of FEM is the magnetic vector potential value at each node of the mesh, whereas in the case of SAIM, the unknowns are the values of the surface currents at the ends of each element.

TABLE III
SUMMARY OF CALCULATION TIMES USED BY FEM AND SAIM

Parameter	FEM	SAIM	Ratio FEM/SAIM
Total number of elements	112 827	1 370	82.36
Total number of degrees of freedom	225 795	2 744	82.29
Const. Discrt. Assemb. Solv. Eq. (s)	112.17	10.05	11.16
Calculation of par. of interest (s)	67.94	5.30	12.82
Total t. (s)	180.11	15.35	11.74

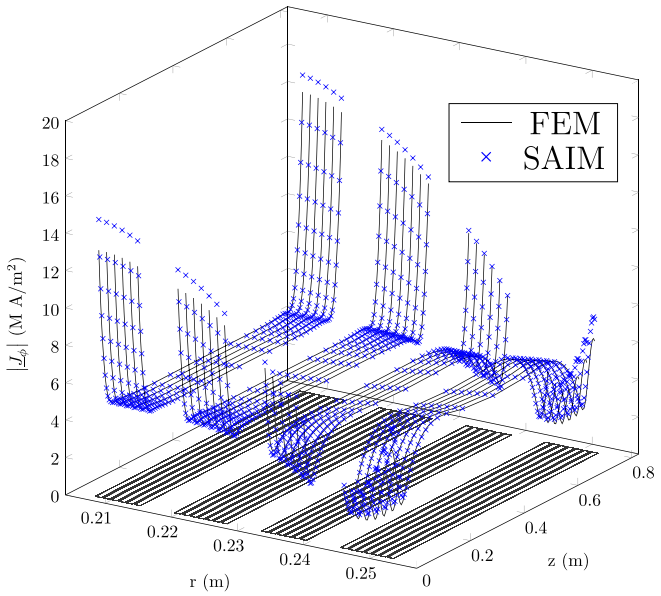

Fig. 9. Current density in the foil conductor winding.

The third row of Table III shows the required computing time for geometry construction, discretization, assembling, and solving the system of equations. The fourth row shows the time spent on calculating the parameters of interest, and the last row reports the total simulation time.

Fig. 9 shows the current distribution in each turn in the foil winding. The results obtained with FEM are plotted in solid line, whereas the ones from SAIM are plotted in blue x labels. The plot shows an inhomogeneous current distribution, showing values several times larger at the ends of the first turn compared with the value of the central part. Excellent agreement between the results of FEM and SAIM can also be appreciated.

V. CONCLUSION

A new methodology for low-frequency magnetic modeling of transformers having foil conductor windings has been proposed in this paper. The proposed methodology has shown a much better computational performance than FEM, being the computation time acceleration factor of about 11 times in a typical case study retaining a reasonable degree of accuracy in the calculation of the current distribution and losses.

The equivalent representation of the transformer components proposed in this paper has the advantage that the discretization is performed only on the interface between two different materials. This means a drastic reduction in the size of the problem and, therefore, in the computation time required with respect to numerical solution methods such as FEM, which require a complete discretization of the problem domain.

On the other hand, unlike FEM, the proposed method naturally represents the outer boundary of the problem, so there is no need to discretize empty space or to apply special considerations related to the boundary condition to be used on the outer boundary.

It should be noted that one of the most important aspects that differentiates SAIM from other integral methods like Boundary Element Method (BEM) or Method of Moments (MOM), is that in the case of SAIM, integral equations are solved in advance without having to take the boundary conditions into account, while in BEM and MOM boundary conditions are an intrinsic part of the integral equation.

It can be finally said that SAIM can be applied to the modeling of transformers having any winding type, such as disk or helical windings.

REFERENCES

[1] B. S. Ram, "Loss and current distribution in foil windings of transformers," *IEE Proc.-Generat., Transmiss. Distrib.*, vol. 145, no. 6, pp. 709–716, Nov. 1998.
[2] P. Solin, I. Dolezel, P. Karban, and B. Ulrych, *Integral Methods in Low-Frequency Electromagnetics*. New York, NY, USA: Wiley, 2009.
[3] P.-B. Zhou, *Numerical Analysis of Electromagnetic Fields*. Berlin, Germany: Springer-Verlag, 1993.
[4] Y. Cheng and Y. Shu, "A new analytical calculation of the mutual inductance of the coaxial spiral rectangular coils," *IEEE Trans. Magn.*, vol. 50, no. 4, Apr. 2014, Art. ID 7026806.
[5] J. Martinez, S. Babic, and C. Akyel, "On evaluation of inductance, DC resistance, and capacitance of coaxial inductors at low frequencies," *IEEE Trans. Magn.*, vol. 50, no. 7, Jul. 2014, Art. ID 8401012.
[6] D. Vanoost, H. De Gersem, J. Peuteman, G. Gielen, and D. Pissoort, "Two-dimensional magnetostatic finite-element simulation for devices with a radial symmetry," *IEEE Trans. Magn.*, vol. 50, no. 5, May 2014, Art. ID 7400204.
[7] N. Mullineux, J. R. Reed, and I. J. Whyte, "Current distribution in sheet- and foil-wound transformers," *Proc. Inst. Elect. Eng.*, vol. 116, no. 1, pp. 127–129, Jan. 1969.
[8] M. M. El-Missiry, "Current distribution and leakage impedance of various types of foil-wound transformers," *Proc. Inst. Elect. Eng.*, vol. 125, no. 10, pp. 987–992, Oct. 1978.
[9] J. A. Ferreira, "Improved analytical modeling of conductive losses in magnetic components," *IEEE Trans. Power Electron.*, vol. 9, no. 1, pp. 127–131, Jan. 1994.
[10] V. Zúbek, "Eddy current losses in transformer low voltage foil coils," *J. Elect. Eng.*, vol. 56, nos. 3–4, pp. 95–99, 2005.
[11] M. T. Villén, J. Letosa, A. Nogués, and R. Murillo, "Procedure to accelerate calculations of additional losses in transformer foil windings," *Electr. Power Syst. Res.*, vol. 95, pp. 85–89, Feb. 2013. [Online]. Available: http://www.sciencedirect.com/science/article/pii/S0378779612002490
[12] S. Salon, B. Lamattina, and K. Sivasubramaniam, "Comparison of assumptions in computation of short circuit forces in transformers," *IEEE Trans. Magn.*, vol. 36, no. 5, pp. 3521–3523, Sep. 2000.
[13] H. E. Knoepfel, *Magnetic Fields: A Comprehensive Theoretical Treatise for Practical Use*. New York, NY, USA: Wiley, 2008.
[14] G. A. Díaz, E. E. Mombello, and V. Stephan, "Magnetic vector potential and magnetic field intensity due to a finite current carrying cylinder considering a variable current density along its axial dimension," *Int. J. Appl. Electromagn. Mech.*, vol. 40, no. 2, pp. 133–147, 2012.
[15] G. A. Díaz and E. E. Mombello, "Magnetic field due to a finite current carrying disk considering a variable current density along its radial dimension," *Int. J. Appl. Electromagn. Mech.*, vol. 42, no. 1, pp. 119–136, 2013.
[16] S. V. Kulkarni and S. A. Khaparde, *Transformer Engineering: Design and Practice*. Boca Raton, FL, USA: CRC Press, 2004.
[17] R. M. Del Vecchio, B. Poulin, P. T. Feghali, D. M. Shah, and R. Ahuja, *Transformer Design Principles: With Applications to Core-Form Power Transformers*. Boca Raton, FL, USA: CRC Press, 2010.